

# A test of the asteroseismic $\nu_{\max}$ scaling relation for solar-like oscillations in main-sequence and sub-giant stars

H. R. Coelho<sup>1,2\*</sup>, W. J. Chaplin<sup>1,2</sup>, S. Basu<sup>3</sup>, A. Serenelli<sup>4</sup>, A. Miglio<sup>1,2</sup> and D. R. Reese<sup>1,2</sup>

<sup>1</sup> School of Physics & Astronomy, University of Birmingham, Edgbaston, Birmingham, B15 2TT, UK

<sup>2</sup> Stellar Astrophysics Centre (SAC), Department of Physics and Astronomy, Aarhus University, Ny Munkegade 120, DK-8000 Aarhus C, Denmark

<sup>3</sup> Department of Physics and Astronomy, Yale University, P.O. Box 208101, New Haven, CT, 06520, USA

<sup>4</sup> Instituto de Ciencias del Espacio (ICE-CSIC/IEEC) Campus UAB, Carrer de Can Magrans, s/n 08193 Cerdanyola del Vallés, Spain

25 May 2015

## ABSTRACT

Large-scale analyses of stellar samples comprised of cool, solar-like oscillators now commonly utilize the so-called asteroseismic scaling relations to estimate fundamental stellar properties. In this paper we present a test of the scaling relation for the global asteroseismic parameter  $\nu_{\max}$ , the frequency at which a solar-like oscillator presents its strongest observed pulsation amplitude. The classic relation assumes that this characteristic frequency scales with a particular combination of surface gravity and effective temperature that also describes the dependence of the cut-off frequency for acoustic waves in an isothermal atmosphere, i.e.,  $\nu_{\max} \propto gT_{\text{eff}}^{-1/2}$ . We test how well the oscillations of cool main-sequence and sub-giant stars adhere to this relation, using a sample of asteroseismic targets observed by the NASA *Kepler* Mission. Our results, which come from a grid-based analysis, rule out departures from the classic  $gT_{\text{eff}}^{-1/2}$  scaling dependence at the level of  $\approx 1.5$  percent over the full  $\approx 1560$  K range in  $T_{\text{eff}}$  that we tested. There is some uncertainty over the absolute calibration of the scaling. However, any variation with  $T_{\text{eff}}$  is evidently small, with limits similar to those above.

## Key words:

asteroseismology – methods: data analysis

## 1 INTRODUCTION

Cool main-sequence and sub-giant (i.e., solar-type) stars display solar-like oscillations, pulsations that are stochastically excited and intrinsically damped by near-surface convection. The solar-like excitation mechanism gives rise to a rich spectrum of detectable oscillations. Data on global (or average) asteroseismic parameters associated with the observed, rich oscillations spectra provide important diagnostics of fundamental stellar properties. Extracting these global parameters from oscillation spectra is usually very straightforward, meaning a large number of stars can easily be analysed. This can be particularly advantageous when low S/N ratios either obstruct or prevent a more detailed analysis of individual modes in the spectrum. Moreover, detailed analysis of stars with high S/N or complicated oscillation spectra can be very time consuming.

Two global asteroseismic parameters have received particular attention, and wide use. One parameter is the average large frequency separation,  $\Delta\nu$ . It is an average of the observed frequency spacings between consecutive overtones  $n$  of the same angular (spherical) degree,  $l$ . The average large separation scales to a very good approximation as  $\rho^{1/2}$ , where  $\rho \propto M/R^3$  is the mean density of

a star of mass  $M$  and surface radius  $R$  (e.g. see Tassoul 1980, Ulrich 1986, Christensen-Dalsgaard 1993). This scaling has physical justification (e.g., see Reese et al. 2012). The second parameter,  $\nu_{\max}$ , is the frequency at which detected modes of a star show the strongest amplitude. Brown et al. (1991) speculated that this characteristic frequency might scale with the atmospheric cut-off frequency for acoustic waves,  $\nu_{\text{ac}}$ . Adopting an isothermal approximation to the full equation describing the cut-off frequency, one derives the scaling  $\nu_{\text{ac}} \propto \nu_{\max} \propto gT_{\text{eff}}^{-1/2}$  (Brown et al. 1991, Kjeldsen & Bedding 1995). Numerous studies have shown empirically that  $\nu_{\max}$  appears to follow this relation to reasonable approximation (e.g., Chaplin & Miglio 2013 and references therein). While some headway has been made on understanding the exact form of the scaling (e.g., Belkacem et al. 2011), a full theoretical justification remains elusive. Additions to the scaling, for example a dependence on the changing Mach number of the near-surface turbulent flow (Belkacem et al. 2013), have also been proposed.

Information encoded in  $\Delta\nu$  and  $\nu_{\max}$  is commonly exploited by using the above scaling dependencies normalized to observed solar parameters or properties, i.e.,

$$\Delta\nu \simeq \left(\frac{M}{M_{\odot}}\right)^{1/2} \left(\frac{R}{R_{\odot}}\right)^{-3/2} \Delta\nu_{\odot} \quad (1)$$

\* E-mail: hugorco@bison.ph.bham.ac.uk

and

$$\nu_{\max} \simeq \left( \frac{M}{M_{\odot}} \right) \left( \frac{R}{R_{\odot}} \right)^{-2} \left( \frac{T_{\text{eff}}}{T_{\text{eff} \odot}} \right)^{-1/2} \nu_{\max \odot}. \quad (2)$$

Typical solar values for the seismic parameters (e.g., see Chaplin et al. 2014) are  $\Delta\nu_{\odot} = 135.1 \mu\text{Hz}$  and  $\nu_{\max \odot} = 3090 \mu\text{Hz}$ . These solar-calibrated scaling relations represent two equations in two unknowns when an estimate of  $T_{\text{eff}}$  is also available, allowing us to solve directly for  $M$  and  $R$  to give so-called “direct” estimates of the stellar properties. Moreover, each relation can be used independently to provide direct estimates of the mean stellar density  $\rho$  (Equation 1) or the surface gravity  $g$  (Equation 2). Alternatively, the relations may be utilized (together or separately) as part of a grid-based search code. Here, one searches amongst a grid of stellar evolutionary models to find those models whose predicted asteroseismic or atmospheric parameters match the actual observed parameters (at the level of the observational uncertainties). The solar-calibrated relations provide the means to translate model properties ( $R$ ,  $M$ ,  $T_{\text{eff}}$ ) to expected values for  $\Delta\nu$  and  $\nu_{\max}$ , thereby allowing a comparison to be made with the observations.

These global asteroseismic parameters and their associated scaling relations are now being employed in analyses of large samples of solar-like oscillators to, for example, generate catalogues of asteroseismic stellar properties (e.g., see Huber et al. 2013, Chaplin et al. 2014, Casagrande et al. 2014, Pinsonneault et al. 2014). Tests in the literature of the scaling relations for solar-type stars have, by and large, returned encouraging results. Studies have most commonly looked at data on estimated stellar radii, and include comparisons with very accurate properties from binaries, parallaxes and long baseline interferometry (e.g., Bruntt et al. 2010, Bedding 2011, Miglio 2012, Huber et al. 2012, Silva Aguirre et al. 2012, White et al. 2013). Results have tested the combination of the two scaling relations to levels of around 4 per cent in inferred radii, and 10 per cent in inferred masses (Chaplin et al. 2014).

Results on red giants are more complicated. For example, Helium core burning and H-shell burning giants with the same mass and radius can have a different  $\Delta\nu$ , due to differences in the sound-speed profile in the outer layers (Miglio et al. 2012), which implies a different absolute scaling for Equation 1. Meanwhile, other studies have looked at open clusters in the *Kepler* field, comparing results on red giants inferred from asteroseismology and from turnoff eclipsing binaries (Broggaard et al. 2012, Sandquist et al. 2013).

Our goal in this paper is to test, empirically, the accuracy of the classic  $\nu_{\max}$  scaling relation for oscillations seen in solar-type stars, i.e., cool main-sequence and sub-giant stars (we leave a study of giants to future work). There is actually very little in the literature on the  $\nu_{\max}$  scaling alone, which partly reflects the difficulty of obtaining the data needed to test the one relation in isolation. A recent example made use of interferometric data on a few very bright *Kepler* targets: White et al. (2013) concluded that results on the F-type star  $\theta$  Cyg may point to problems for the  $\nu_{\max}$  scaling in the hottest solar-type stars.

Our basic approach is as follows. We use data on a sample of around 500 stars observed by the NASA *Kepler* Mission (the same sample as in Chaplin et al. 2014). Each star in our sample has a measured  $\nu_{\max}$ , which comes from analysis of the *Kepler* data. Throughout the rest of the paper we shall refer to these actual, measured values as  $\nu_{\max}(\text{data})$ . Now, the classic scaling relation (Equation 2) gives  $\nu_{\max}$  in terms of  $g$  and  $T_{\text{eff}}$ , or, to be more specific, the combination  $g T_{\text{eff}}^{-1/2}$ . We can therefore test the scaling if we have independent measures of

$$\nu_{\max}(\text{grid}) \equiv \left( \frac{g}{g_{\odot}} \right) \left( \frac{T_{\text{eff}}}{T_{\text{eff} \odot}} \right)^{-1/2} \nu_{\max \odot}, \quad (3)$$

to which the observed  $\nu_{\max}(\text{data})$  may be compared. The  $\nu_{\max}(\text{grid})$  are so-named because we adopt a grid-based search technique to estimate them, using as inputs the asteroseismic average large separations,  $\Delta\nu$ , of the stars along with photometric temperatures,  $T_{\text{eff}}$ , derived using the Infrared Flux Method (IRFM) and, where available, metallicities  $[\text{Fe}/\text{H}]$  from spectroscopy. We search grids of stellar evolutionary models to find those models whose predicted  $\{\Delta\nu, T_{\text{eff}}, [\text{Fe}/\text{H}]\}$  match the actual observed inputs. Each model in the grid also has a computed  $\nu_{\max}(\text{grid})$ , which comes from its  $M$ ,  $R$  and  $T_{\text{eff}}$ . The best-matching models will have the most likely values of  $\nu_{\max}(\text{grid})$ . A suitable, likelihood-weighted average therefore provides an estimate of  $\nu_{\max}(\text{grid})$  for every star (see Section 3.2), which may then be compared directly to the observed  $\nu_{\max}(\text{data})$ . Any departures from a one-to-one correspondence of the values would point to problems with the classic scaling relation, and allow us to quantify departures from the scaling. In sum, we leverage the potential of using asteroseismic results on a large number of solar-type stars to follow a statistical (ensemble) approach to the analysis and to thereby beat-down the errors. The approach is not dissimilar to that adopted by Morel et al. (2014) for part of their analysis of red giants observed by the CNES/ESA CoRoT Mission, which compared values of the surface gravity estimated using  $\Delta\nu$  on the one hand and  $\nu_{\max}$  on the other.

The layout of the rest of the paper is as follows. We begin in Section 2 with a discussion of the basic methodology adopted to test the  $\nu_{\max}$  scaling relation. Section 3 then introduces the real *Kepler* data, the artificial data we made to check our methodology (Section 3.1), and the grid-based search pipelines used to estimate the  $\nu_{\max}(\text{grid})$  values (Section 3.2). Our results are presented in Section 4, beginning with a validation of the methodology using artificial data (Section 4.1), followed by results from the actual *Kepler* sample. We finish in Section 5 with concluding remarks.

## 2 METHOD

We may in principle use some suitable grid-based results to test the  $\nu_{\max}$  scaling relation, albeit with caveats that we will discuss and address below. Let us suppose for the moment that grid-based searches using the set of inputs

$$\{\Delta\nu, T_{\text{eff}}, [\text{Fe}/\text{H}]\}$$

provide robust, unbiased estimates of the combination  $g T_{\text{eff}}^{-1/2}$ , as calibrated to give  $\nu_{\max}(\text{grid})$  defined by Equation 3 above. Assuming the temperatures and metallicities to be unbiased, at least to a level that will not influence significantly estimation of the combination  $g T_{\text{eff}}^{-1/2}$ , the fractional differences

$$[\nu_{\max}(\text{data})/\nu_{\max}(\text{grid})] - 1,$$

will provide a direct estimate of the bias in the  $\nu_{\max}$  scaling, i.e., the fractional amount by which the  $\nu_{\max}(\text{data})$  values are over or underestimated relative to  $(g/g_{\odot})(T_{\text{eff}}/T_{\text{eff} \odot})^{-1/2} \nu_{\max \odot}$ .

Crucial to the approach is the accuracy of  $\nu_{\max}(\text{grid})$ . First, we know to expect a small bias if the grid-based search pipelines employ the  $\Delta\nu$  scaling relation, as we now go on to explain. When the scaling relation is used in the grid-based searches, the fundamental properties of models in the grid are used as inputs to Equation 1 to yield model estimates of  $\Delta\nu$  for comparison with the observed separations. Alternatively, one may circumvent use of the scaling

by computing for each model a set of theoretical oscillation frequencies (e.g., radial-mode frequencies spanning the same orders as those observed in the real data), from which one may then estimate the required  $\Delta\nu$  from a suitable fit to those frequencies.

It is now well known that predictions made by the calibrated scaling-relation (Equation 1) have small, systematic differences with respect to predictions from model-computed frequencies (e.g., see Ulrich 1986, White et al. 2011; Mosser et al. 2013). For solar-type stars, these differences can be up to  $\approx 2$  percent in size, and become more pronounced at effective temperatures progressively further away from  $T_{\text{eff}} \approx 5700$  K (e.g., see Figures 5 and 6 of White et al. 2011; and figures in Chaplin et al. 2014). Here, we have employed grid-based search pipelines that can run with or without the  $\Delta\nu$  scaling relation. We use one pipeline that may be run either using individual model-calculated frequencies or the  $\Delta\nu$  scaling relation; and, for comparison, two other pipelines that used the  $\Delta\nu$  scaling only.

Second, we must consider the impact of the poor modelling of the near-surface layers of stars. In the case of the Sun it is now well established that this gives rise to a frequency-dependent offset between observed and model-calculated oscillation frequencies (e.g., see Chaplin & Miglio 2013, and references therein). This so-called “surface term” increases in magnitude with increasing overtone number,  $n$ . The amount by which  $\Delta\nu$  is affected will depend on the variation of the surface term with  $n$ . Tests of the grid-based method (Basu et al. 2010) indicate that the impact of the solar surface term on  $\Delta\nu$  – which decreases the observed solar  $\Delta\nu$  by just under 1 per cent compared to model predictions – leads only to very small errors in the inferred solar properties, certainly well within the observational uncertainties associated with the *Kepler* data used in this paper. Stellar surface terms would need to be substantially larger than the solar term to produce significant bias in our results. However, the nature of the term in other stars remains rather poorly understood, and so this caveat should be borne in mind.

Our tests with artificial data do nevertheless provide some insights on the sensitivity of the results to such offsets. The artificial data come from models computed using a different stellar evolutionary code and different input physics to those of the grids to which the grid-based pipelines are coupled. This can give rise to “surface-term” like offsets between models in the artificial sample in the grids that share the same fundamental properties (in particular from differences in boundary conditions, matching to model atmospheres etc.).

### 3 DATA AND GRID PIPELINES

#### 3.1 Real and artificial data

The observational data for our study come from Chaplin et al. (2014). This study produced an asteroseismic catalogue from an extensive grid-based analysis of more than 500 solar-like oscillators, which were observed by *Kepler* as part of an asteroseismic survey that was conducted over the first 10 months of science operations. Stellar properties were estimated from a grid-based analysis using the global asteroseismic parameters  $\Delta\nu$  and  $\nu_{\max}$  together with complementary photometric and spectroscopic data as the inputs. Homogeneous sets of effective temperatures  $T_{\text{eff}}$  were available for the full sample of stars, courtesy of complementary ground-based photometry. A homogeneous set of spectroscopic parameters ( $T_{\text{eff}}$  and  $[\text{Fe}/\text{H}]$ ) was also available from Bruntt et al. (2012), but only for a subset of 87 stars in the sample

Here, we make use of the global asteroseismic parameters and the complementary data to perform the new grid-based analysis needed to test the  $\nu_{\max}$  scaling relation. The Chaplin et al. (2014) sample is dominated by cool main-sequence and sub-giant stars but does contain a small fraction of stars at the base of the red-giant branch that were serendipitously observed as part of the short-cadence asteroseismic survey. We have removed the more evolved stars from the sample (which will be the subject of a separate study). The selected sample contains 426 solar-type stars.

As noted above, complementary photometry was available on the entire sample. This allowed us to perform a new, homogenous grid-based analysis on all the selected solar-type stars, but at the cost of not having robust, well-constrained estimates of  $[\text{Fe}/\text{H}]$  for each star since the complementary photometry available to us in the *Kepler* Input Catalogue (KIC; see Brown et al. 2011) does not provide strong constraints on metallicity. Just like Chaplin et al. (2014), we therefore adopted an average  $[\text{Fe}/\text{H}]$  value as input for every star when we analysed the 426-star sample. We actually tried two different values: One set of results came from using the average of the 87 metallicities measured by Bruntt et al. (2012), i.e.,  $[\text{Fe}/\text{H}] = -0.05$  dex; while the other results came from using  $[\text{Fe}/\text{H}] = -0.20$  dex for all stars (e.g., see Silva Aguirre et al. 2011), the value adopted in Chaplin et al. (2014). In both cases we adopted large input uncertainties of  $\pm 0.3$  dex.

In spite of the weak constraints on  $[\text{Fe}/\text{H}]$ , we still obtained more precise results from the larger 426-star sample having complementary photometric data than we did from the smaller sample with complementary spectroscopic data because the larger sample size compensated for the inferior precision in  $[\text{Fe}/\text{H}]$ . Results obtained were similar, and hence in what follows we present detailed results from the photometric sample. This sample also provided much better coverage in the domain where  $T_{\text{eff}} > 6000$  K.

Finally with regards to the input data, we note that the photometric temperatures were the Infrared Flux Method (IRFM) estimates from Chaplin et al. (2014), which were calculated using multi-band photometry in the Two Micron All Sky Survey (2MASS; see Skrutskie et al. 2006) JHK bands, and in the Sloan Digital Sky Survey (SDSS) *griz* bands (both available in the KIC).

Panel (a) of Fig. 1 plots the locations of the sample of selected *Kepler* solar-type stars on a Hertzsprung-Russell diagram. The lines mark evolutionary tracks computed by the Modules for Experiments in Stellar Astrophysics (MESA) code (Paxton et al. 2011; see below), for models having solar composition and masses ranging from  $0.8$  to  $1.5 M_{\odot}$  (in steps of  $0.1 M_{\odot}$ ). Panel (b) of the same figure shows the measured  $\nu_{\max}(\text{data})$  of the *Kepler* sample, from analysis of the oscillation spectra of the stars, indicating the parameter range tested by the analysis.

We also used artificial data to test and validate our methodology. The artificial sample of stars was comprised of models drawn from an evolutionary grid, computed using MESA. The grid spanned the range  $0.8 \leq M/M_{\odot} \leq 1.5$  and  $-0.8 \leq [\text{Fe}/\text{H}] \leq 0.8$  (both in steps of  $0.1$ ), with tracks computed from the pre-main sequence to the base of the red-giant branch.

The Grevesse & Noels (1993) value of  $Z_{\odot}/X_{\odot} = 0.0245$  was used to translate between model values of  $[\text{Fe}/\text{H}]$  and  $Z/X$ . The OPAL equation of state (Rogers & Nayfonov 2002) and OPAL opacities (Iglesias & Rogers 1996) were used, augmented by low-temperature opacities from Ferguson et al. (2005). Nuclear reaction rates were from NACRE (Angulo et al. 1999), with updates for the  $^{14}\text{N}(p, \gamma)^{15}\text{O}$  (Imbriani et al. 2004, 2005) reaction. Convection was treated according to mixing-length theory, using the solar-calibrated mixing length parameter. Diffusion and effects of

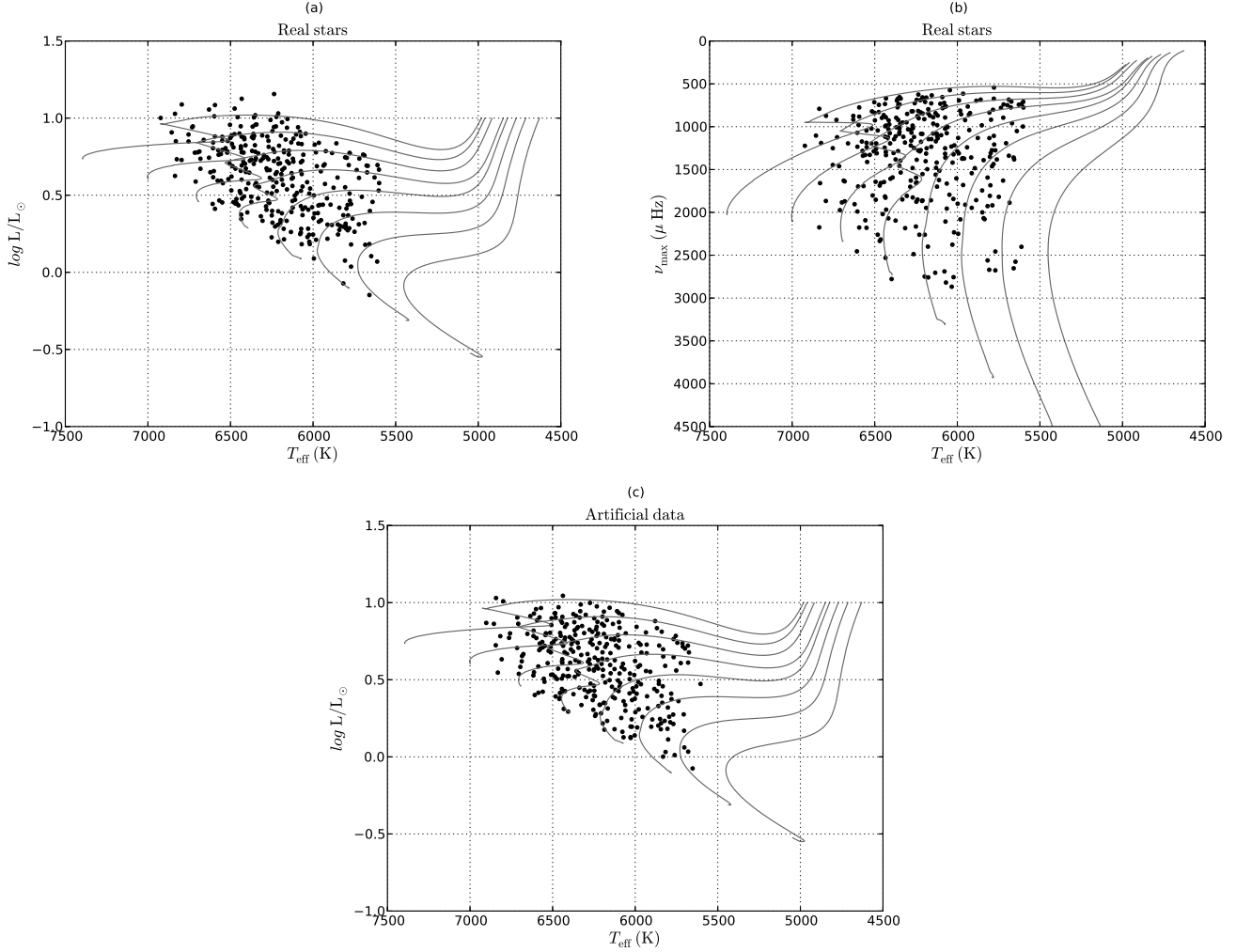


**Figure 1.** Panel (a): Hertzprung-Russell diagram of the asteroseismic sample of *Kepler* solar-type stars. Panel (b): measured values,  $\nu_{\text{max}}(\text{data})$ , from analysis of the oscillation spectra of the real stars, also as a function of effective temperature. Panel (c): Hertzprung-Russell diagram of the sample of artificial targets, computed from MESA models. The lines in the panels show evolutionary tracks computed by the MESA code (see text), for models having solar composition and masses ranging from 0.8 to 1.5  $M_{\odot}$  (in steps of 0.1  $M_{\odot}$ ).

rotational mixing were not included. The primordial Helium abundance was fixed to  $Y_p = 0.2484$  (Cyburt et al. 2003), and the helium enrichment set to  $\Delta Y/\Delta Z = 2$  (e.g., Chiosi & Matteucci 1982, Carigi & Peimbert 2008). We refer the reader to Paxton et al. (2011) for further details.

Artificial stars were drawn from the grid by seeking a “best matching” model for each of the solar-type stars in the *Kepler* sample (via a  $\chi^2$  minimization). We found that a selection based solely on a comparison of the observed (*Kepler*) and model (grid) values of  $T_{\text{eff}}$  and  $\Delta\nu$  (the latter using the calibrated scaling relation) was sufficient to produce an artificial sample that had distributions in each of the fundamental properties that were a reasonable match to those for the real sample. Panel (c) of Fig. 1 marks the locations of the selected models in our artificial sample of stars (using the pristine model parameters). Owing to the limited resolution of the grid, we found that some real stars had the same best-matching artificial model. This meant that our final sample of selected artificial stars was comprised of 306 unique models.

Next, we computed adiabatic oscillation frequencies for each of the 306 selected models, using the GYRE (Townsend & Teitler

2013) stellar oscillations code. The  $\Delta\nu$  of each artificial star was then given by the best-fitting gradient of a linear fit to the radial order,  $n$ , of the five  $l = 0$  frequencies centred on the estimated  $\nu_{\text{max}}$  (see below) of the model. This approach gives values that are representative of the average values extracted from the real data. We also tested the impact of calculating  $\Delta\nu$  using a different number of orders (to reflect the varying data quality and S/N levels in the real sample of stars) and from adopting a weighted fit of the frequencies (to reflect the impact of the changing S/N in any given observed spectrum). Neither change had a significant impact on our results.

We computed three different sets of  $\nu_{\text{max}}$  for the artificial sample. One set was computed assuming perfect adherence to the solar-calibrated scaling relation, i.e., by using Equation 2. We made two other sets by applying a temperature-dependent fractional offset to the solar-calibrated scaling relation, i.e., a computation that took the form

$$\nu_{\text{max}} = \mathcal{F}(T_{\text{eff}}) \left( \frac{M}{M_{\odot}} \right) \left( \frac{R}{R_{\odot}} \right)^{-2} \left( \frac{T_{\text{eff}}}{T_{\text{eff},\odot}} \right)^{-1/2} \nu_{\text{max},\odot}, \quad (4)$$

with  $\mathcal{F}(T_{\text{eff}})$  being the fractional temperature-dependent offset. We

applied a linear and quadratic offset, respectively, both of which are shown in panel (a) of Fig. 4 (in the figure that also shows results from the data; see below for further discussion). Use of the first set of “perfect” values allowed us to test the impact of biases not associated with the  $\nu_{\max}$  scaling relation; while the other sets allowed us to test whether we could recover information on a known bias in the  $\nu_{\max}$  scaling.

Finally, with each artificial star then having calculated values of  $\Delta\nu$  and  $\nu_{\max}$ , and a model  $T_{\text{eff}}$ , it remained to add noise and to assign uncertainties to those parameters for input to the grid pipelines. This meant that in our analysis we would treat the artificial data in exactly the same way as the real data. Here, we simply used the relevant parameter uncertainties of the real *Kepler* star to which each artificial star was associated. To make a given realization of the artificial datasets, we added Gaussian noise to each pristine input parameter, multiplied by the relevant parameter uncertainty, to give  $\nu_{\max}(\text{data})$ ,  $\Delta\nu(\text{data})$ , and  $T_{\text{eff}}(\text{data})$  for each artificial star.

### 3.2 Grid pipelines

We utilized three different grid-based pipeline codes to return estimates of the parameter  $\nu_{\max}(\text{grid})$  for all stars in the real and artificial samples:

- the Bellaterra Stellar Properties Pipeline (BeSPP) (Serenelli et al. 2013, extended for asteroseismic modelling);
- the Yale-Birmingham (YB) (Basu et al. 2010, 2012, Gai et al. 2011); and
- PARAM (da Silva et al. 2006; Miglio et al. 2013; Rodrigues et al. 2014);

The BeSPP pipeline was run with a grid comprised of models constructed with the GARSTEC code (Weiss & Schlattl 2008). The parameters of the grid are described in Silva Aguirre et al. (2012). BeSPP was run in two different modes of operation: one where grid-model estimates of  $\Delta\nu$  were computed using adiabatic oscillation frequencies (frequency mode); and one where the estimates were instead computed using the solar-calibrated scaling relation (Equation 1; scaling-relation mode). The other two pipelines were run only in the latter, scaling-relation mode. PARAM was run using a grid comprising models made by the Padova group (Marigo et al. 2008). Further details may be found in Miglio et al. (2013). The YB pipeline returned results using five different sets of stellar models: grids computed by the Dartmouth (Dotter et al. 2008) and Padova groups (Bressan et al. 2012); the set of YY isochrones (Demarque et al. 2004); a grid comprised of the BASTI models of Pietrinferni et al. (2004), computed for use in asteroseismic studies (see Silva Aguirre et al. 2013); and, finally, a grid constructed using the YREC Code (Demarque et al. 2008), which is described by Basu et al. (2012). This grid has been used in other papers, and we retain the YREC2 name here.

We also report results from YB which are labelled ALL. This set of results was generated by combining the YB analysis over all five grids to compute what are in essence averages from a composite “super distribution”. This is a new addition to the YB code that has not previously been documented in the literature, and so we provide further details here.

The YB pipeline determines the properties of a star using the given observational input (central) parameter set. A key step in the method is to generate 10,000 input parameter sets by adding different random realisations of Gaussian noise (commensurate with the input uncertainties) to the actual (central) observational input parameter set. For each realisation, we find all models in a grid

within  $3\sigma$  of the input uncertainties, and use these models to define a likelihood function (e.g., see Gai et al. 2011, Basu et al. 2012 for details). The estimated property, e.g.,  $\nu_{\max}(\text{grid})$ , is then the likelihood-weighted average of the property of the selected models. The 10001 values of any given property estimated from the central value and the 10000 realisations, form the probability distribution function for that parameter. In the YB pipeline we adopt the median of the distribution as the estimated value of the property, and we use  $1\sigma$  limits from the median as a measure of the uncertainties. The ALL results were obtained by constructing a consolidated probability distribution for a given star by adding together the five different distribution functions obtained using the five different grids. Then we determined the median of this consolidated or “super” distribution function, to determine the average  $\nu_{\max}(\text{grid})$ .

All three pipelines were employed in the grid-based analysis described in Chaplin et al. (2014), where summary details of the physics employed in the grids may also be found.

## 4 RESULTS

### 4.1 Results from artificial data

We begin with results from analysing the first set of artificial data. Recall that in this case  $\nu_{\max}(\text{data})$  for each artificial star – essentially the proxy for what would be the observed  $\nu_{\max}$  of each real star – was computed assuming strict adherence to the solar-calibrated scaling relation. The top two panels of Fig. 2 show results from the BeSPP pipeline, run in both frequency mode [panel (a)] and scaling-relation mode [panel (b)], on a representative noise realization of the artificial set. Both panels show fractional differences  $\nu_{\max}(\text{data})/\nu_{\max}(\text{grid}) - 1$ , i.e., fractional differences between the simulated measurements,  $\nu_{\max}(\text{data})$ , and the grid-based estimates,  $\nu_{\max}(\text{grid})$ . Here, grid-based estimates were calculated assuming an input [Fe/H] pegged to the Bruntt et al. average, i.e., [Fe/H] =  $-0.05$  dex. Results are shown both for the individual artificial stars (symbols) and for averages computed over 130-K bins in  $T_{\text{eff}}$  (lines). The error bars mark uncertainties on each average. The scatter in the fractional differences is entirely consistent with the formal uncertainties on the differences (which are propagated from the individual formal uncertainties on  $\nu_{\max}(\text{data})$  and  $\nu_{\max}(\text{grid})$ ).

The results on the whole show the expected trends. The scaling-relation-mode results in panel (b) are not flat. The differences show an upward trend with increasing  $T_{\text{eff}}$ , which is due to the known offsets in the  $\Delta\nu$  scaling. This tells us that if there were no  $\nu_{\max}$  bias in the real data we should expect to see trends like these when using a scaling-relation-based grid pipeline.

With regards to the frequency-mode results in the panel (a) of Fig. 2, as expected the upward trend from the  $\Delta\nu$  scaling is absent, and we see a flat trend in the comparison at the level of precision of the data. The frequency-mode results therefore allow us to conclude, correctly, that the artificial data follow a  $gT_{\text{eff}}^{-1/2}$  like scaling. That said, the differences do show a small absolute offset, albeit one that does not change significantly with  $T_{\text{eff}}$ . The absolute offset has more than one contribution.

First, there is a contribution due to the uncertainty in [Fe/H] we adopted for the input data (to mimic that for the real 426-star sample). Panel (c) of Fig. 2 shows results from BeSPP run in frequency mode, but with [Fe/H] =  $-0.20$  dex now used as input for all stars. This change to the input [Fe/H] produces a shift in the absolute offset of just under 1 per cent. Second, there will be a contribution to the absolute offset arising from differences between the

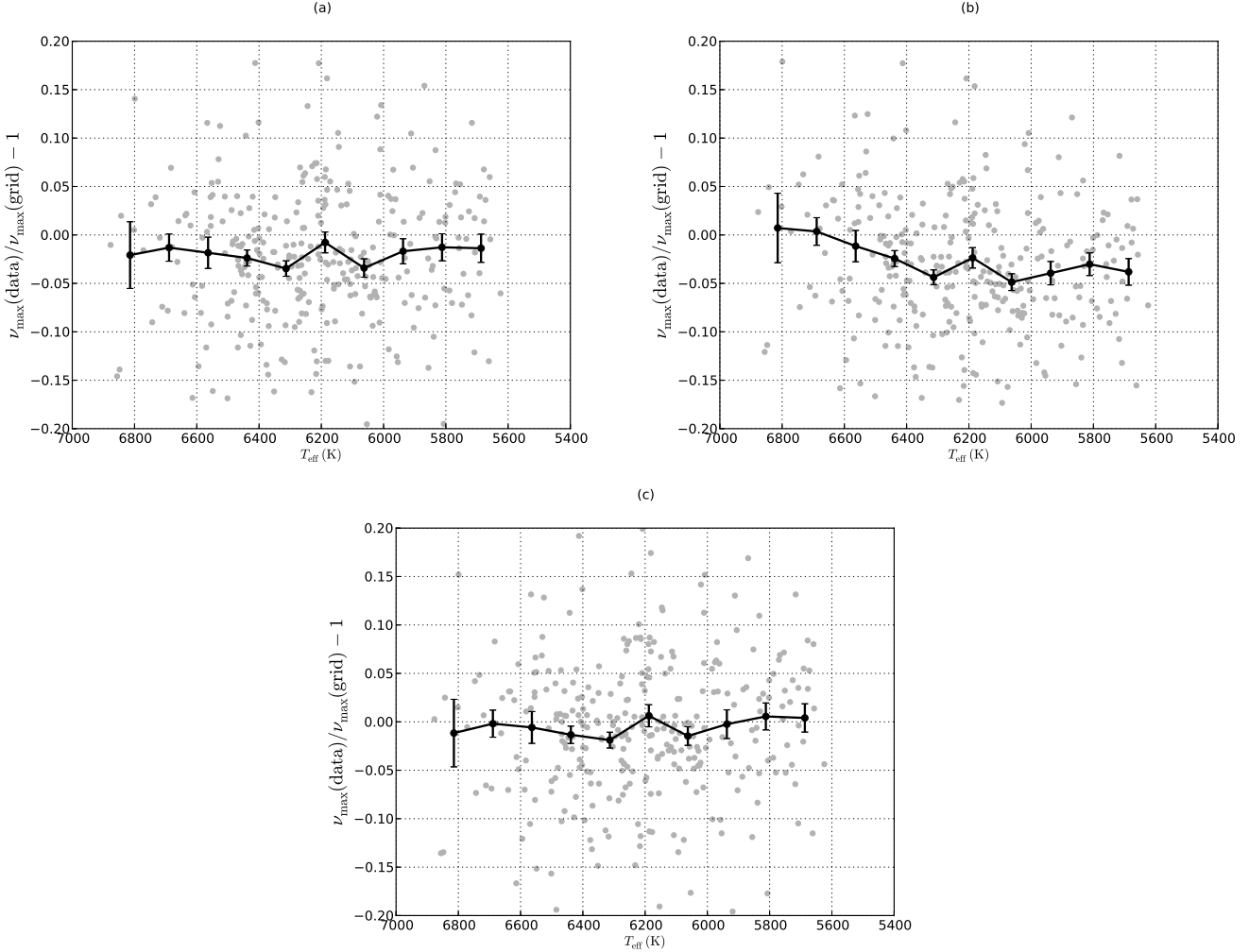


**Figure 2.** Results from BeSPP grid pipeline, for artificial data following perfect adherence to the  $\nu_{\max}$  scaling relation. Panel (a) shows results from when BeSPP is run in frequency mode; while panel (b) shows results when the pipeline is run in scaling-relation mode (see text). Plotted are fractional differences  $\nu_{\max}(\text{data})/\nu_{\max}(\text{grid}) - 1$ , with grid-based estimates calculated assuming an input  $[\text{Fe}/\text{H}]$  of  $-0.05$  dex for every artificial star. Results are plotted for individual artificial stars (symbols) and for averages computed over 130-K bins in  $T_{\text{eff}}$  (lines). The error bars mark uncertainties on each average. Panel (c): Frequency-mode results from analysing the same artificial data, but now with an input  $[\text{Fe}/\text{H}]$  of  $-0.20$  dex.

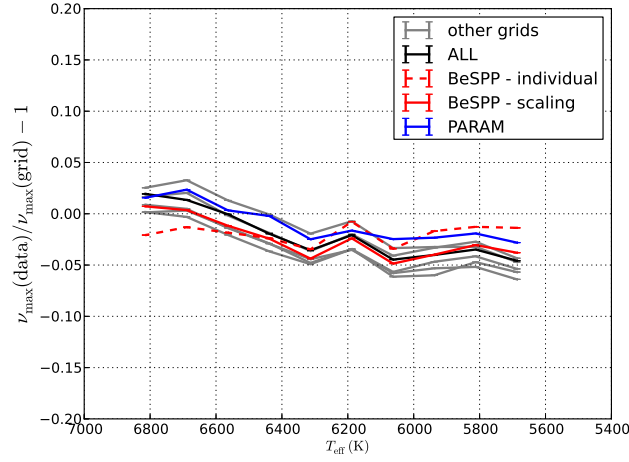
models on which the artificial stars are based and those used in the BeSPP grid. These differences can give rise to what looks like a “surface term” offset (see discussion in Section 2 above). We conclude that we should expect there to be some uncertainty over the *absolute* calibration of the relation for results on the real *Kepler* data. We shall come back in Section 4.2 to attempt an estimate of the relative contributions of the above effects to the uncertainty in the absolute calibration.

Fig. 3 also includes results from the YB and PARAM pipelines, which were coupled to a variety of grids with  $[\text{Fe}/\text{H}] = -0.05$  dex used as input. The YB ALL results are plotted in black, the YB results from individual grids in grey, and the PARAM results in blue. Recall that these pipelines were run only in scaling-relation mode. To aid the clarity of the plots we present just the  $T_{\text{eff}}$ -binned averages. Results from the other pipelines follow the BeSPP scaling-relation results from the top panels of Fig. 2, which we plot again here (in red) for direct comparison. The shapes of the scaling-relation trends for each grid-pipeline combination are similar – showing an upward trend with increasing  $T_{\text{eff}}$ , again due

to the known offsets in the  $\Delta\nu$  scaling – with an extreme spread of approximately 3.5 per cent in the fractional differences.

Fig. 4 presents results for the artificial sets which have known biases in  $\nu_{\max}$ . Panel (a) shows the linear and quadratic biases,  $\mathcal{F}(T_{\text{eff}})$  (Equation 4), which we imposed on the artificial data. The other panels show results of testing the biased artificial data, with fractional differences plotted for each biased set (see figure legends). Also plotted for reference (black lines) are the recovered trends from the unbiased data (see Figs. 2 and 3). The panels show returned fractional differences from: BeSPP in frequency mode (b); BeSPP run in scaling mode (c); YB ALL (d); and PARAM (e).

The results are again encouraging. Evidence of the injected bias is clearly present in the results. We also see the offset between the two bias trends, although we would not be able to tell the difference between the shapes of the trends. Nevertheless, we are able to conclude that for the level of bias tested here, it would be possible to discriminate between the no-bias and bias cases.



**Figure 3.** Fractional differences  $\nu_{\max}(\text{data})/\nu_{\max}(\text{grid}) - 1$  returned by all three grid pipelines, for artificial data following perfect adherence to the solar-calibrated  $\nu_{\max}$  scaling relation (Equation 2). Different lines show 130-K averages in  $T_{\text{eff}}$  for different pipeline-grid combinations (see annotation), all of which used an input  $[\text{Fe}/\text{H}]$  of  $-0.05$  dex.

## 4.2 Results from *Kepler* data

Fig. 5 shows results from analysing the selected sample of *Kepler* solar-type stars, which all have complementary photometric data. The fractional differences  $\nu_{\max}(\text{data})/\nu_{\max}(\text{grid}) - 1$  are plotted for the different pipelines, including results obtained using BeSPP in both modes of operation. The top four panels show results with  $[\text{Fe}/\text{H}] = -0.05$  dex used as input, as returned by: BeSPP in frequency mode (a); BeSPP run in scaling mode (b); YB ALL (c); and PARAM (d).

The trends observed here bear a striking resemblance to those given by the results on the artificial data that follow the classic  $\nu_{\max}$  scaling relation. The trend in the BeSPP frequency-mode *Kepler* results on the real data is flat in  $T_{\text{eff}}$ , and consistent with a  $gT_{\text{eff}}^{-1/2}$  like scaling at the level of precision of the data.

The scatter in the fractional differences of the real data in Fig. 5 is entirely consistent with statistical scatter, given the formal uncertainties. The histograms in Fig. 6 show the normalized distributions of fractional differences for the real (red) and artificial no-bias (blue) BeSPP frequency-mode results. Here, each  $\nu_{\max}(\text{data})/\nu_{\max}(\text{grid}) - 1$  was subtracted from the respective mean trend-line of its sample, and then normalized by its formal uncertainty, that uncertainty having been propagated from the individual formal uncertainties on  $\nu_{\max}(\text{data})$  and  $\nu_{\max}(\text{grid})$ . The lines show the cumulative distributions of the histogram data. The real and artificial data histograms follow one another very closely.

We may quantify further the adherence of the BeSPP frequency-mode results to a  $gT_{\text{eff}}^{-1/2}$  like scaling, i.e., a flat trend. If we fit a simple linear model to *all* the data, the best-fitting gradient implies a linear bias of  $0.16 \pm 0.10$  per cent per 100 K. We may therefore rule out departures from a  $gT_{\text{eff}}^{-1/2}$  scaling at the level of  $\approx 1.5$  percent over the full  $\Delta T \approx 1560$  K range tested in  $T_{\text{eff}}$ .

As noted in Section 1, the scaling relations (Equations 1 and 2) may be manipulated to give expressions for the stellar radius,  $R$ , and mass,  $M$ . The dependencies of the resulting expressions imply that any bias in  $\nu_{\max}$  propagates to give bias in the inferred properties of

and

$$\left(\frac{\delta M}{M}\right) = 3 \left(\frac{\delta \nu_{\max}}{\nu_{\max}}\right).$$

Departures from the classic scaling of  $\approx 1.5$  percent across the full range (see above) therefore fix 1- $\sigma$  upper limits on changes in any bias in inferred properties with changing  $T_{\text{eff}}$  of  $\delta R/R \leq 1.5$  percent and  $\delta M/M \leq 4.5$  percent. Since the  $\nu_{\max}$  scaling relation implies

$$\left(\frac{\delta g}{g}\right) = \left(\frac{\delta \nu_{\max}}{\nu_{\max}}\right),$$

bias in surface gravities inferred from use of the relation will be similar to that for the radii above (which corresponds to a bias in  $\log g$  of  $\approx 0.006$  dex).

We also fitted data in overlapping  $\Delta T_{\text{eff}} = 500$  K-wide bins, moving systematically through the full range to test the temperature dependence of any departures from the scaling. Throughout most of the range we obtain 1- $\sigma$  uncertainties on the best-fitting gradients of  $\approx 0.4$  per cent per 100 K. The limits increase to  $\approx 0.5$  per cent per 100 K at temperatures above about 6200 K, rising to  $\approx 1$  per cent per 100 K in the highest range we fitted, which started at 6450 K.

Our results nevertheless imply some uncertainty over the *absolute* calibration of the  $\nu_{\max}$  scaling. Panel (e) in Fig. 5 shows the impact on the BeSPP frequency-mode results of using a different input  $[\text{Fe}/\text{H}]$  for each star, here  $-0.20$  dex instead of the value of  $-0.05$  dex used for the top left-hand panel. Just like the artificial data in Fig. 2, we see a systematic shift in the absolute offset, from just over 3 per cent for an input  $[\text{Fe}/\text{H}]$  of  $-0.05$  dex to around 4 per cent for an input  $[\text{Fe}/\text{H}]$  of  $-0.20$  dex. Assuming that the overall shift results from the quadratic addition of uncorrelated effects, this implies a systematic shift due to the uncertainty in  $[\text{Fe}/\text{H}]$  of around 2.5 per cent. It is worth noting that if we analyse the smaller sample of real stars having spectroscopic data from Bruntt et al. (2012) – which have much more tightly constrained input  $[\text{Fe}/\text{H}]$  – we get the same  $\approx 3$  per cent offset as the  $-0.05$  dex full-sample case.

Accounting for the above still leaves us with an uncertainty in the absolute calibration of around 3 per cent (again, assuming that the contributions are uncorrelated). We recall from discussions in previous sections that we would expect this to reflect differences

$$\left(\frac{\delta R}{R}\right) = \left(\frac{\delta \nu_{\max}}{\nu_{\max}}\right),$$

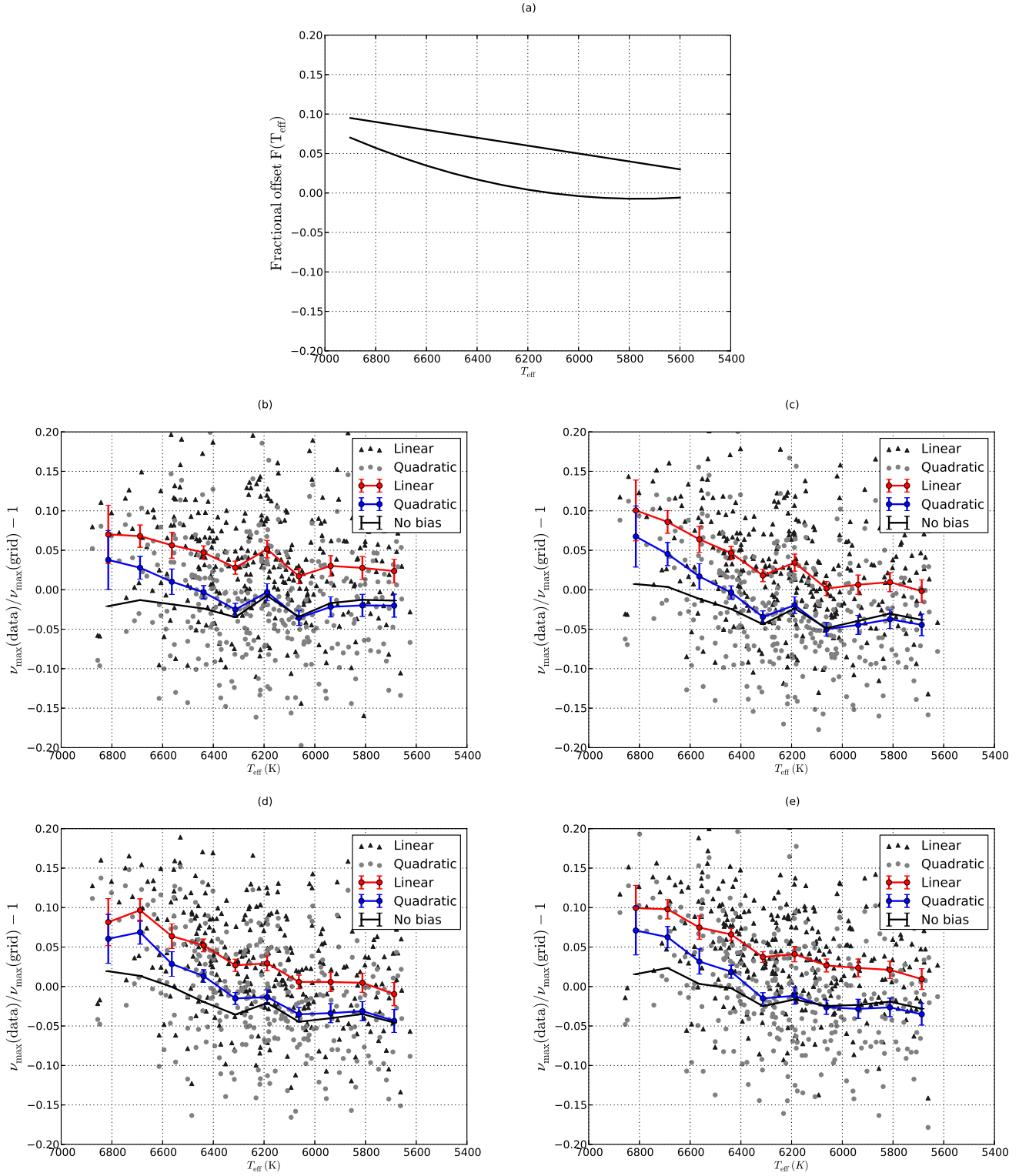


**Figure 4.** Results from all grid pipelines, using an input  $[\text{Fe}/\text{H}]$  of  $-0.05$  dex, for artificial datasets having a  $T_{\text{eff}}$ -dependent bias imposed on the solar-calibrated  $\nu_{\text{max}}$  scaling relation. Panel (a): Linear and quadratic biases,  $\mathcal{F}(T_{\text{eff}})$  (Equation 4), imposed on the artificial data. Other panels: results of testing the biased artificial data. Plotted are the fractional differences  $\nu_{\text{max}}(\text{data})/\nu_{\text{max}}(\text{grid}) - 1$  for each biased set, returned by: BeSPP in frequency mode (b); BeSPP run in scaling mode (c); YB ALL (d); and PARAM (e). Each panel also shows for comparison the result from the unbiased data (see Figs. 2 and 3).



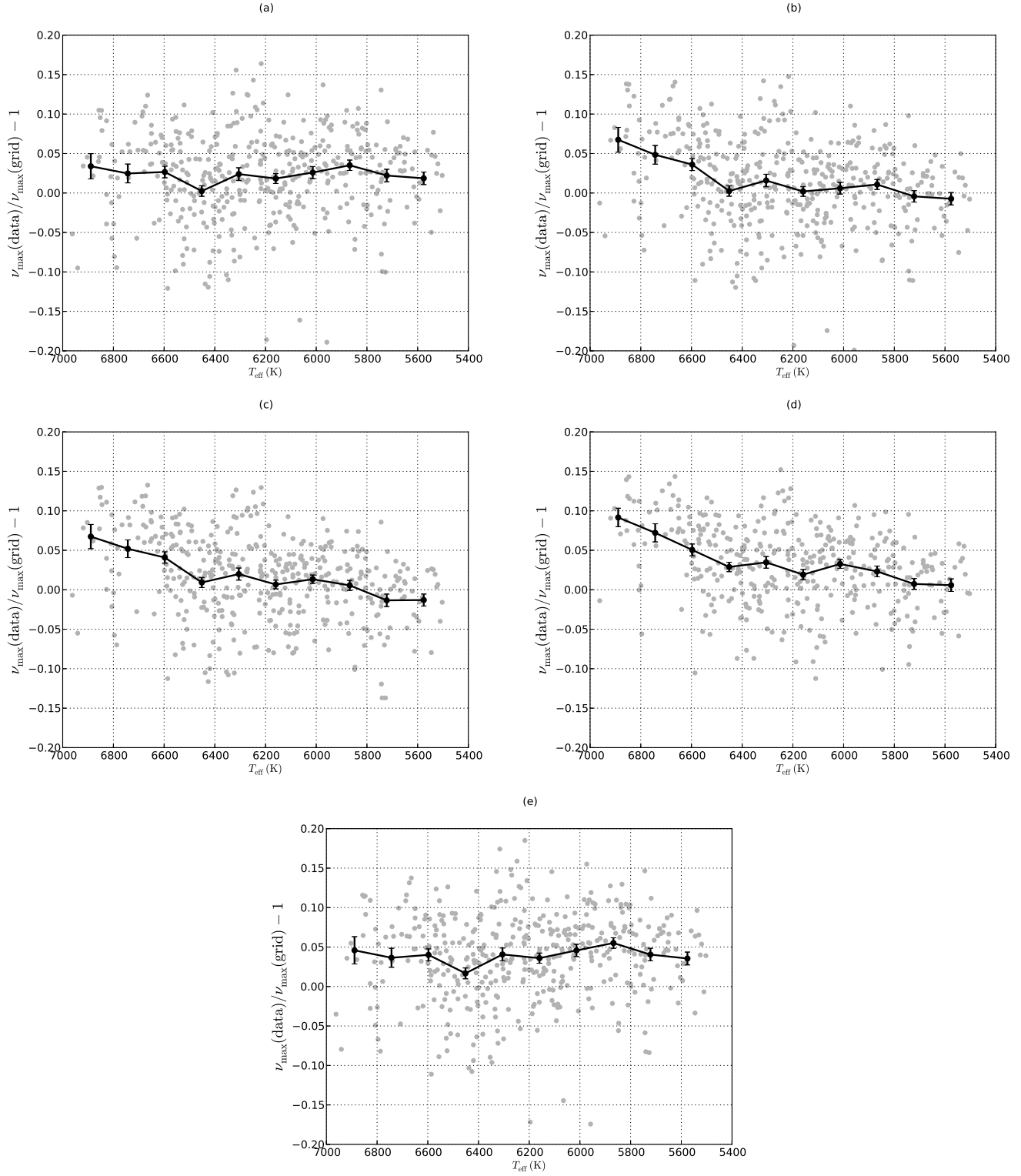


**Figure 5.** Results from analysis of the real *Kepler* sample of solar-type stars, showing the fractional differences  $\nu_{\max}(\text{data})/\nu_{\max}(\text{grid}) - 1$  returned by the different pipelines. The top four panels show results with  $[\text{Fe}/\text{H}] = -0.05$  dex used as input, as returned by: BeSPP in frequency mode (a); BeSPP run in scaling mode (b); YB ALL (c); and PARAM (d). Panel (e): BeSPP frequency-mode results form using an input  $[\text{Fe}/\text{H}]$  of  $-0.20$  dex for every star.

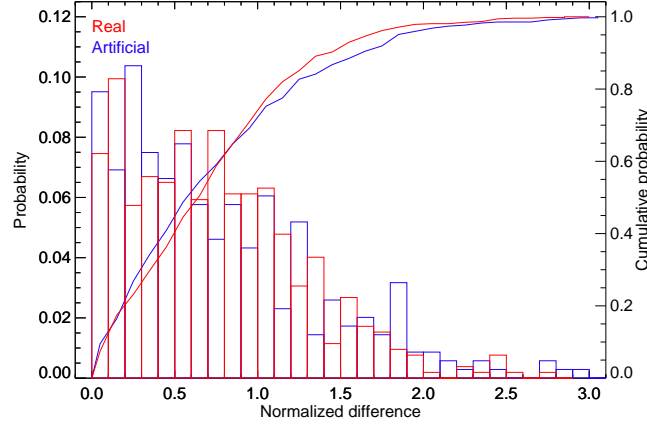


**Figure 6.** Bar plots (associated to left-hand ordinate scale): histograms of the normalized distribution of fractional differences  $\nu_{\max}(\text{data})/\nu_{\max}(\text{grid}) - 1$  for the artificial no-bias (blue) and real (red) BeSPP frequency-mode results, which were plotted in Figs. 2 and 5 respectively. Each fractional difference was subtracted from the respective mean trend-line of its sample, and then normalized by its formal uncertainty, that uncertainty having been propagated from the individual formal uncertainties on  $\nu_{\max}(\text{data})$  and  $\nu_{\max}(\text{grid})$ . Lines (associated to right-hand ordinate scale): the cumulative distributions of the histogram data.

between the physics and structures of the real stars (including near-surface effects) and those of the grid models.

An analysis performed on  $\Delta T_{\text{eff}} = 500 \text{ K}$ -wide bins finds no evidence for any significant deviation of the offset with  $T_{\text{eff}}$ . The results imply that if there are any absolute errors in the calibration, all inferred properties will be biased by the *same* fractional amount. For the solar-calibrated Equation 2 the calibration is provided by the value  $\nu_{\max\odot} = 3090 \mu\text{Hz}$ . Guided by the results above, a 3 per cent uncertainty in the overall calibration translates to an error in the the calibrating frequency of around  $100 \mu\text{Hz}$ .

## 5 CONCLUSION

Asteroseismic scaling relations for solar-like oscillators are becoming increasingly important as they receive more widespread use in building large catalogues of stellar properties.

We have tested the scaling relation for the global asteroseismic parameter  $\nu_{\max}$ , the frequency at which a solar-like oscillator presents its strongest observed pulsation amplitude. The classic scaling relation assumes that  $\nu_{\max}$  scales with surface gravity and effective temperature according to  $gT_{\text{eff}}^{-1/2}$ . We have tested how well the detected oscillations in a large sample of solar-type stars observed by the NASA *Kepler* Mission adhere to this relation by comparing the observed  $\nu_{\max}$  of the stars with independent estimates of the combination  $gT_{\text{eff}}^{-1/2}$ .

Our results rule out departures from the classic  $\nu_{\max}$  scaling at the level of  $\approx 1.5$  percent over the full  $\approx 1560 \text{ K}$  range in  $T_{\text{eff}}$  that we tested. There is some uncertainty over the absolute calibration of the scaling, but any variation with  $T_{\text{eff}}$  is evidently small, with limits similar to those above.

## ACKNOWLEDGMENTS

The authors would like to thank L. Girardi and T. S. Rodrigues for use of the most recent PARAM code. Funding for this Discovery mission is provided by NASA's Science Mission Directorate. The authors wish to thank the entire *Kepler* team, without whom these results would not be possible. The research leading to these results has received funding from the the UK Science and

Technology Facilities Council (STFC) and the European Community's Seventh Framework Programme ([FP7/2007-2013]) under grant agreement no. 312844 (SPACEINN). H.R.C. acknowledges support from grant BEX 8569/12-6 (CAPES/Birmingham). Funding for the Stellar Astrophysics Centre is provided by The Danish National Research Foundation (Grant agreement no.: DNR106). S.B. acknowledges partial support from NSF grant AST-1105930 and NASA grant NNX13AE70G. A.M.S. is partially supported by grants ESP2013-41268-R (MINECO) and 2014SGR-1458 (Generalitat of Catalunya).

## REFERENCES

- Basu, S., Chaplin, W. J., Elsworth, Y., 2010, *ApJ*, 710, 1596
- Basu, S., Verner, G. A., Chaplin, W. J., Elsworth, Y. 2012, *ApJ*, 746, 76
- Bedding TR. 2014. In *Asteroseismology*, Canary Islands Winter School of Astrophysics, Vol. 23, eds. P. L. Pall'è, C. Esteban. Cambridge, UK: Cambridge Univ. Press, p. 60
- Belkacem, K., Goupil, M. J., Dupret, M. A., et al, 2011, *A&A*, 530, 142
- Belkacem, K., Samadi, R., Mosser, B., Goupil, M.-J., Ludwig, H.-G., 2013, *ASPC*, 479, 61
- Bressan, A. Marigo, P., Girardi, L., Salasnich, B., Dal Cero, C., Rubele, S., Nanni, A., 2012, *MNRAS*, 427, 127
- Brown, T. M., Gilliland, R. L., Noyes, R. W., Ramsey, L. W., 1991, *ApJ*, 368, 599
- Brown, T. M., Latham, D. W., Everett, M. E., Esquerdo, G. A. 2011, *AJ*, 142, 111
- Brogaard, K., VandenBerg, D. A., Bruntt, H., et al., 2012, *A&A*, 543, A106
- Bruntt, H., Bedding, T. R., Quirion, P. O., et al. 2010, *MNRAS*, 405, 1907
- Bruntt, H., Basu, S., Smalley, B., et al. 2012, *MNRAS*, 423, 122
- Carigi, L., Peimbert, M., 2008, *RMxAA*, 44, 341
- Casagrande, L., Ramírez, I., Meléndez, J., et al. 2010, *A&A*, 512, 54
- Casagrande, L., Silva Aguirre, V., Stello, D., et al., 2013, *ApJ*, 787, 110

- Chaplin, W. J., Houdek, G., Appourchaux, T., et al. 2008, *A&A*, 485, 813
- Chaplin, W. J., Miglio, A., 2013, *ARAA*, 51, 353
- Chaplin, W. J., Basu, S., Huber, D., et al., 2014, *ApJS*, 210, 1
- Chiosi, C., Matteucci, F. M., 1982, *A&A*, 105, 140
- Christensen-Dalsgaard, J. 1993, *Proc. GONG 1992, Seismic Investigation of the Sun and Stars (ASP Conf. Ser. 42)*, ed. T. M. Brown (San Francisco, CA: ASP), p. 347
- Cyburt, R. H., Fields, B. D., Olive, K. A., *Phys. Lett. B.*, 567, 227
- da Silva L., et al., 2006, *A&A*, 458, 609
- Demarque, P., Woo, J.-H., Kim, Y.-C., Yi, S. K. 2004, *ApJS*, 155, 667
- Dotter, A., et al. 2008, *ApJS*, 178, 89
- Gai, N., Basu, S., Chaplin, W. J., Elsworth, Y., 2011, *ApJ*, 730, 63
- Grevesse, N., Noels, A., 1993, *PhST*, 47, 133
- Huber, D., Ireland, M. J., Bedding, T. R., et al., 2012, *ApJ*, 760, 32
- Huber, D., Chaplin, W. J., Christensen-Dalsgaard, J., et al., 2013, *ApJ*, 767, 127
- Kjeldsen, H., Bedding, T. R., 1995, *A&A*, 293, 87
- Miglio, A., 2012, in: *Red Giants as Probes of the Structure and Evolution of the Milky Way*. Berlin: Springer, Miglio, A., Montalbán J., Noels, A., eds., p. 11
- Miglio, A., Brogaard, K., Stello, D., et al., 2012, *MNRAS*, 419, 2077
- Miglio, A., Chiappini, C., Morel, T., et al., 2013, *MNRAS*, 429, 423
- Morel, T., Miglio, A., Lagarde, N., et al., 2014, *A&A*, 564, 119
- Mosser, B., Michel, E., Belkacem, K., et al., 2013, *A&A*, 550, 126
- Paxton, B., Bildsten, L., Dotter, A., et al., 2011, *ApJS*, 192, 3
- Pietrinferni, A., Cassisi, S., Salaris, M., & Castelli, F. 2004, *ApJ*, 612, 168
- Pinsonneault, M. H., An, D., Molenda-Żakowicz, J., et al. 2012, *ApJS*, 199, 30
- Pinsonneault, M. H., Elsworth, Y., Epstein, C., et al. 2014, *ApJS*, 215, 19
- Reese, D. R., Marques, J. P., Goupil, M. J., Thompson, M. J., Deheuvels, S., 2012, *A&A*, 539, 63
- Rodrigues, T. S., Girardi, L., Miglio, A., et al., 2014, *MNRAS*, 445, 2758
- Sandquist, E. L., Mathieu, R. D., Brogaard, K., et al., 2013, *ApJ*, 762, 58
- Serenelli, A. M., Bergemann, M., Ruchti, G., Casagrande, L., 2013, *MNRAS*, 429, 3645
- Silva Aguirre, V., Chaplin, W. J., Ballot, J., et al. 2011, *ApJL*, 740, L2
- Silva Aguirre, V., Casagrande, L., Basu, S., et al. 2012, *ApJ*, 757, 99
- Silva Aguirre, V., Basu, S., Brandão, I. M., et al. 2013, *ApJ*, 769, 141
- Skrutskie, M. F., Cutri, R. M., Stiening, R., et al. 2006, *AJ*, 131, 1163
- Tassoul, M., 1980, *ApJS*, 43, 469
- Townsend, R. H. D., Teitler, S. A., 2013, *MNRAS*, 435, 3406
- Ulrich R. K., 1986, *ApJ*, 306, L37
- White, T. R., Bedding, T. R., Stello, D., Christensen-Dalsgaard, J., Huber, D., Kjeldsen, H., 2011, *ApJ*, 743, 161
- White, T. R., Huber, D., Maestro, V., et al., 2013, *MNRAS*, 433, 1262